Separation Science and Technology
Publication details, including instructions for authors and subscription information:
http://www.informaworld.com/smpp/title~content=t713708471

Experimental Investigation into the Filtration and Reverse Flow Cleaning Modes on Cylindrical and Tapered Rigid Ceramic Filters

T. G. Chuah[a]; C. J. Withers[b]; J. P. K. Seville[c]
[a] Department of Chemical and Environmental Engineering, Faculty of Engineering, Universiti Putra Malaysia, Selangor D.E., Malaysia [b] Caldo Environmental Engineering Ltd., Worcester, United Kingdom [c] Department of Chemical and Formulation Engineering, School of Engineering, The University of Birmingham, Edgbaston, Birmingham, United Kingdom

Online publication date: 08 July 2010

SEPARATION SCIENCE AND TECHNOLOGY
Vol. 39, No. 16, pp. 3797–3820, 2004

Experimental Investigation into the Filtration and Reverse Flow Cleaning Modes on Cylindrical and Tapered Rigid Ceramic Filters

T. G. Chuah,[1,*] C. J. Withers,[2] and J. P. K. Seville[3]

[1]Department of Chemical and Environmental Engineering, Faculty of Engineering, Universiti Putra Malaysia, Serdang, UPM, Selangor D.E., Malaysia
[2]Caldo Environmental Engineering Ltd., Worcester, United Kingdom
[3]Department of Chemical and Formulation Engineering, School of Engineering, The University of Birmingham, Edgbaston, Birmingham, United Kingdom

ABSTRACT

This paper describes the equipment test facility and setup that has been developed in the laboratory and the investigation into both the filtration and reverse flow modes of low-density rigid ceramic filters at ambient conditions. The purpose is to study the fluid behavior by conducting experiments to investigate the pressure drop and the velocity profile

*Correspondence: T. G. Chuah, Department of Chemical and Environmental Engineering, Faculty of Engineering, Universiti Putra Malaysia, Serdang, UPM, 43400, Selangor D.E., Malaysia; E-mail: chuah@eng.upm.edu.my.

DOI: 10.1081/SS-200041073 0149-6395 (Print); 1520-5754 (Online)

along a filter element. Two different ceramic filter media were used in the majority of this work. Cerafil XS-1000 is the current product from Cerel (cylindrical) and the tapered filter, which is a novel design of the ceramic filter tailor made for this study. Both the filtration and reverse flow cleaning results suggest that a more uniform pressure generation is found in tapered filters than it is the cylindrical filters. The origin of nonuniformity in pressure difference across the wall, in both the filtration and cleaning modes, is internal (axial) pressure drop that can be reduced by reducing the axial gas velocity, which obviously takes its highest value towards the open end (in both filtration and cleaning modes).

Key Words: Rigid ceramic filters; Filtration; Reverse flow; Pressure drop; Tapered filters.

INTRODUCTION

Many industrial processes involve the generation of hot gases, which can be contaminated with either solid, liquid, or gaseous pollutants. Environmental legislation enacted as a result of government policy has compelled industry to pay serious attention to the air pollution issue. Particulate emission limits for a variety of processes in Malaysia[1] are shown in Table 1. High-temperature, high-pressure particle control is essential to meet both

Table 1. Environmental quality (clean air) regulation, Malaysia, 1978.[1]

Substances emitted	Standards		
1. Solid particles concentration in the heating of metals	Standard A: 0.3 g/m^3 Standard B: 0.25 g/m^3 Standard C: 0.2 g/m^3		
2. Solid particles concentration in other operations	Standard A: 0.6 g/m^3 Standard B: 0.5 g/m^3 Standard C: 0.4 g/m^3		
3. Metals and metallic compounds:	Std. A	Std. B (in unit of g/m^3)	Std. C
• Mercury	0.02	0.01	0.01
• Cadmium	0.025	0.015	0.015
• Lead	0.04	0.025	0.025
• Antimony	0.04	0.025	0.025
• Arsenic	0.04	0.025	0.025
• Zinc	0.15	0.1	0.1
• Copper	0.15	0.1	0.1

environmental and turbine equipment specifications in advanced coal-fired power generation systems. Thus, attention has been given to the removal of the particulate emissions, the most visible sign of pollution.

The frontier in gas filtration is removing particulates from gases at elevated temperatures. In chemical and process industries and in incineration, the need for gas cleaning is being driven increasingly by the requirements of environmental legislation, which has been directed specifically at particulate, acid gases, heavy metal compounds, hydrogen chloride, and organic chlorides such as dioxin and furans. Filtering at higher temperature not only helps to prevent the corrosion problem, it also may improve both thermodynamic efficiency and versatility of the overall process. Moreover, with the cut down of the total power requirement due to lower pressure drop, it is more economic to filter gases hot instead of cold.[2]

Ceramic filters are designed to meet performance, life, and cost constraints of the process application in which they are used. They are a highly effective high-temperature filtration method that possesses excellent resistance to chemical and thermal attack. These filters also prove their strength in showing high particulate removal efficiencies, high flow capability, and relatively low pressure drop characteristics.[2,3] It is usually assumed that the required tensile cleaning stress in a conventional fabric filter is set up primarily by the movement caused by the cleaning pulse. Pulse cleaning displaces the fabric outwards. When it becomes taut, it decelerates sharply, normally at many times gravitational acceleration. The cake then experiences a tensile stress, which depends on its areal density and on the deceleration. If the stress is sufficient, the cake is thrown clear of the medium. Rigid filter media, such as ceramic filters, show no displacement on cleaning. The tensile stress is, therefore, entirely the result of the pressure drop imposed across the cake as a result of the reverse flow of cleaning gas.

Effective cleaning is essential if the conditioning behavior of the filter is to be acceptable; it is clearly important to be able to assess the magnitude of the required cleaning action.[4] Several studies have been carried out on pulse gas cleaning. All these studies have shown that the reverse pulse pressure is not usually uniformly distributed along the filter element. It is generally agreed that the pressure is greatest at the closed end of the candle and at a minimum, or even close to zero, at the open end. Therefore, the cleaning mechanism becomes important in order to achieve better efficiency on dust removal.

Differential pressure measurements along the filter candles have been mostly performed at room temperature.[5–8] Measurements at high temperatures have been described and reported by Berbner and Löffler,[9] Hajek and Peukert,[10] and Ito et al.[11]. Velocity measurements in ceramic filter elements during pulse cleaning have been carried out by Baik et al.,[12] Christ and Renz,[13] and Biffin et al.[14]. Baik et al.[12] found that a new filter candle will exhibit a certain degree of inhomogeneity and has the possibility of blind-

ing (dust cake remaining accumulated on the filter surface). This dust will remain on the candle surface after cleaning. These factors will severely affect the flow within the candle, both under operation and cleaning. Christ and Renz[13] measured the axial velocity with a laser doppler anemometer in order to validate the numerical simulations of a single filter element during pulse cleaning. Biffin et al.[14] measured the axial velocity along the filter candle using a hot-wire probe. In their studies, a larger duration pulse showed no significant influence on the maximum velocity level inside the filter.

EXPERIMENTAL METHODS

To investigate the factors that influence the achievement of a minimum stable operating pressure drop, several variables were investigated on a rig which uses one, horizontally mounted, 60 mm outer diameter candle. The experimental rig is shown schematically in Fig. 1. The single filter rig with the filter house is shown together with the fan, the controller, and the measurement apparatus. The dirty gas entry was 1.4 m above the top of the filter and 0.75 m from its open end. The element was mounted in place by forcing the open end of the filter candle against the header plate. This allowed an excellent seal to be made by using a rubber gasket and a rubber sealant com-

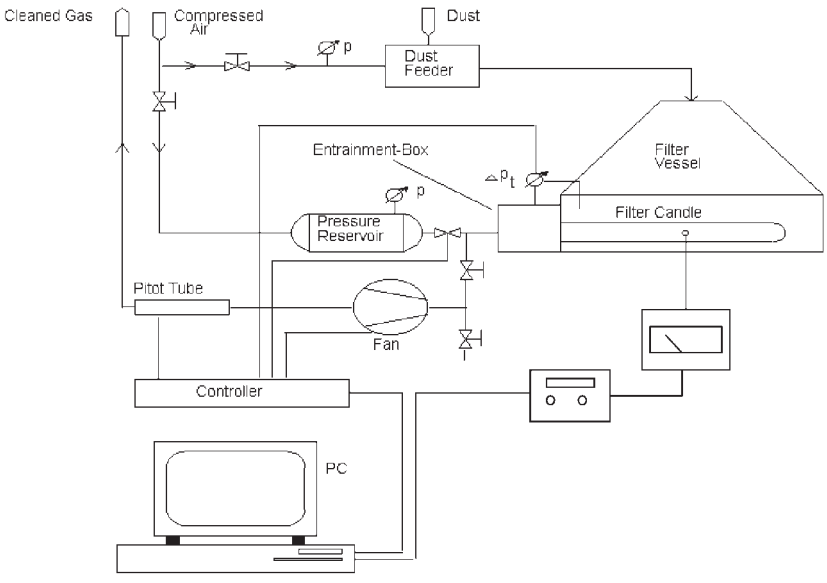

Figure 1. Schematic diagram of the single candle rig.

pound. The filter is clamped horizontally, as mounting filter elements this way has some advantages, most importantly the use of the momentum of the inlet gas to enhance dust settling by forcing it downwards to the filter base. The control of the filter rig was designed to maintain operation at a specified constant face velocity. A proportional-integral-derivative (PID) controller was applied to maintain the mean face velocity by continually adjusting the flowrate of the fan.

The filter rig, which operates at ambient conditions, is used to study the influence of cleaning pressure and areal loading on the residual pressure drop of three proprietary brands of filter element. Two different geometries of ceramic filters will be tested: cylindrical and tapered or conical. It is believed that one way in which the pressure difference generated across the wall of the filter element can be made more uniform along its length is to vary the cross sectional area of the element, most simply by tapering from the open end to the closed end. Hence, experimental studies of tapered filters were undertaken in order to understand the effect of the filter geometry on the pressure difference distribution.

Two different ceramic filter media were used in the majority of this work. Cerafil XS-1000 is the product from Cerel and the tapered filter (as shown in Fig. 2), is a novel design of the ceramic filter tailor made for this study. The properties of both filters are shown in Tables 2 and 3, respectively.

Measurements of Pressure Difference and Average Velocity

a) Filtration

For the filtration operation, a flow of dusty air with the selected overall face velocity was injected into the filter housing from above. The filtration face velocity under ambient pressure and temperature condition ranged from 4 cm/s to 6 cm/s. A PID controller was applied in order to keep the face velocity constant. Static pressure tapings at different sections were taken. Due to the limitation of the experimental rig, the controller could not maintain the flow stability when the mean face velocity was over 6 cm/s. Therefore, in this

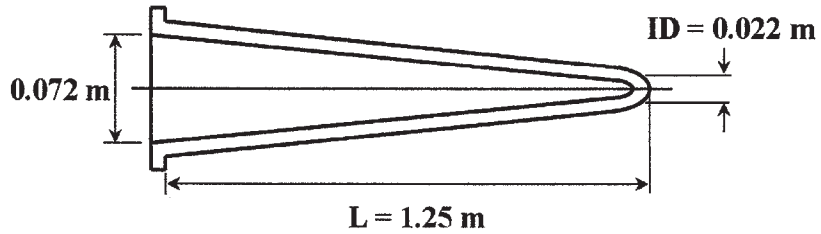

Figure 2. Schematic diagram of the tapered filter.

Table 2. Technical data for Cerafil XS-1000.

Property	Value
Candle length	1000 ± 2 mm
Candle external diameter	60 ± 2 mm
Candle internal diameter	40 ± 2 mm
Filtration area	$0.19\,m^2$
Density	$450 \pm 5\,kg\ m^{-3}$
Porosity	$86 \pm 2\%$
Chemical analysis (after firing) Al_2O_3	43.7% w/w
SiO_2	56.3% w/w
Filtration efficiency	>99.9% w/w*
Temperature limit	900°C

work, the experiment is not carried out with a face velocity higher than 6 cm/s. However, in industrial practice face velocities used are usually not greater than 5 cm/s due to pressure drop limitations.[15]

The pressure was measured at various points along the filter using the taping tubes and a micromanometer. The locations of taping tubes are shown in Figs. 3(a)–(b).

b) Reverse Flow

For the reverse flow experiments, an air flow with selected volumetric flow rate was delivered into the filter candle from the open end as shown in Fig. 4. The desired flow rate was calculated using the orifice equation. A manual control butterfly valve and a micromanometer are used to control the inlet volumetric flow rate entering the filter. The tapings used to measure the pressure drop and average velocity are also described in the following section.

Table 3. Technical data for tapered filter.

Property	Value
Length	1250 ± 2 mm
Filter external diameter (open end)	9.0 ± 2 mm
(closed end)	4.0 ± 2 mm
Filter internal diameter (open end)	40 ± 2 mm
(closed end)	20 ± 2 mm
Porosity	88%
Filtration area	$0.32\,m^2$
Temperature limit	900°C

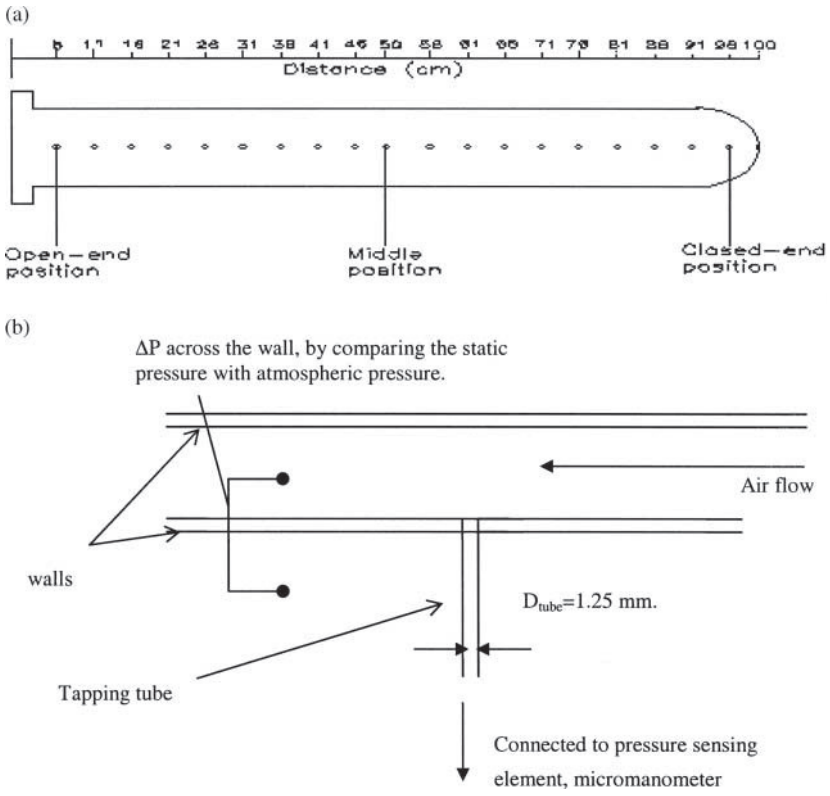

Figure 3. (a) Positions of pressure tappings; (b) measurement of pressure difference.

Average Velocity and Volumetric Measurements

Small steel pressure tapings with an outside diameter of 1.25 mm (O.D. ϕ) and inside diameter of 1 mm (I.D. ϕ) were utilized for the pressure difference and flow rate measurements. Measurements were taken using the procedure recommended by Perry and Green,[16] i.e., at the center of the filter and at three different radii. These radial positions were determined from Eq. (1);

$$\sqrt{\frac{2n-1}{N}} = \frac{r_n}{R} \tag{1}$$

where, N = number points of traverse (for this case, N = 7), n is the order of traverse radius (n = 1, 2, 3, . . . , $N/2$), R = candle inner radius (20 mm), and r_n is traverse radius. The arithmetical mean of the velocities on each radius

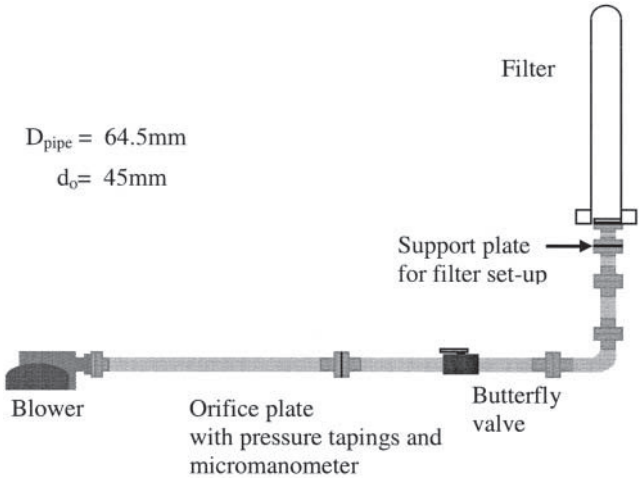

Figure 4. Reverse flow experimental rig.

(exclusive of the center) was taken as the average velocity for the cross section. The assumption in this method is that flow is axis symmetric within the candle, so measurements were only taken on one point for each radius. In order to achieve a better accuracy more measurements should be taken per radius to get a mean velocity per radius as well (British Standard BS1024).[17] Since the wall roughness of the filter interior surface is estimated to be 1 mm,[15] measurements close to the wall would not be expected to be very accurate. For the determination of the volumetric flow rate and the velocity in the filter candle at a cross section, Eqs\. (2) and (3) were used:

$$Q = \sqrt{\frac{2\overline{\Delta P}}{\rho}} \cdot A \tag{2}$$

$$\bar{v} = \sqrt{\frac{2\overline{\Delta P}}{\rho}} \tag{3}$$

where $\overline{\Delta P}$ is the average of the dynamic pressure at the cross section, determined by traversing, ρ is the density of air, and A is the cross-section area of the filter candle, $\pi D^2/4$.

$$\overline{\Delta P} = \frac{P_1 + P_2 + P_3}{3} \tag{4}$$

with P_1, P_2, and P_3 as the local dynamic pressures at measurement points (traverse radius) of 1, 2, and 3.

Reverse Flow Experimental Rig Setup

The experimental rig is shown schematically in Fig. 4. The filter rig for reverse flow is shown together with the blower, the controller valve, and measurement apparatus. An orifice plate inserted in a pipe system causes a pressure drop, ΔP, which can be measured by pressure tapings placed on either side of the plate. This pressure drop is related to the air flow rate, Q, through the pipe system and can be calculated by the equation known as "the orifice equation":[18]

$$\Delta P = \frac{8Q^2\rho(1-\beta^4)}{\pi^2 C^2 \varepsilon_1^2 d_o^4} \tag{5}$$

Rearranging:

$$Q = \sqrt{\frac{\pi^2 C^2 \varepsilon_1^2 d^4 \Delta P}{8\rho(1-\beta^4)}} \tag{6}$$

where β represents the ratio between the orifice diameter, d_o, and the pipe diameter, D_{pipe}.

$$\beta = \frac{d_o}{D_{pipe}} \tag{7}$$

$$\varepsilon_1\left[\frac{P_1 - \Delta P_{orifice}}{P_1} \to 1\right] \approx 0.99 \tag{8}$$

ε_1 is called the expansibility factor, which approaches a value of 1 for negligible pressure drops (when compared to the static pressure, P_1, up stream of the orifice plate), ρ is the density of the fluid. C represents the discharge coefficient of the orifice plate and can be calculated using the following correlation:

$$C = 0.5959 + 0.0312\beta^{2.1} - 0.184\beta^8 + 0.0029\beta^{2.5}\left[\frac{10^6}{Re}\right]^{0.75} + 0.00351L_1 - 0.033L_2'\beta^3 \tag{9}$$

with Reynolds number, Re_D

$$Re = \frac{4Q}{\pi\nu D_{pipe}} \tag{10}$$

ν represents the kinematic viscosity of the fluid. L_1 and L'_2 have values of 1 and 0.47 respectively. These are known as the distance quotients for pressure tapings of type D and D/2 (where D refers to D_{pipe}). Equation (9) has to be solved numerically as the discharge coefficient, C, is a function of the flow rate, Q,

which is the variable of interest. The orifice equation is generally valid in the following parameter range:[18]

$$d_o \geq 12.5\,\text{mm}$$

$$50\,\text{mm} \leq D_{pipe} \leq 1000\,\text{mm}$$

$$0.2 \leq \beta \leq 0.75$$

$$\text{Re} \geq 1260\,\beta^2 D_{pipe}$$

For the equipment used in this study, the pipe diameter, D_{pipe}, equaled 64.5 mm, the diameter of orifice, d_o, was 45 mm, and β was about 0.7. An analogue version micromanometer (Model FC014-5, Furness Controls Ltd., UK) was used to measure the pressure drop induced by an orifice plate in the pipe. The pressure differential measurement range is 0–2000 mm $H_2O \pm 0.5\%$. In order to obtain better accuracy for the pressure difference measurement, an FCO520 AirPro Pressure and Flow Meter (Furness Controls Ltd., UK) was also used to measure both the pressure difference and the flow rate of the reverse flow. It is a microprocessor-based instrument that measures the pressure difference and velocities when paired with pitot tubes. The differential pressure range isthinsp;$\pm$20 kPa and the velocity range is 180 m/s. It possesses an accuracy of 0.25% full scale division (FSD).

RESULTS AND DISCUSSIONS

The effects of face velocity on the pressure difference and axial velocity were investigated experimentally. Filtration face velocities under ambient pressure and temperature conditions, ranged from 4 cm/s to 6 cm/s.

Effect of Face Velocity to Axial Velocity

Schiftner[19] investigated the flow distribution in a 1.5 m BWF KE 85/60 × 1515 ceramic filter element both experimentally and using the model of Clift et al.[15]. The experimental results showed poor agreement with the predictions from the model. He suggested that one possible reason may be the fact that the resistance to flow of the medium is not uniform along the length of the filter element. Measurement method on filter resistance is shown in the Appendix.

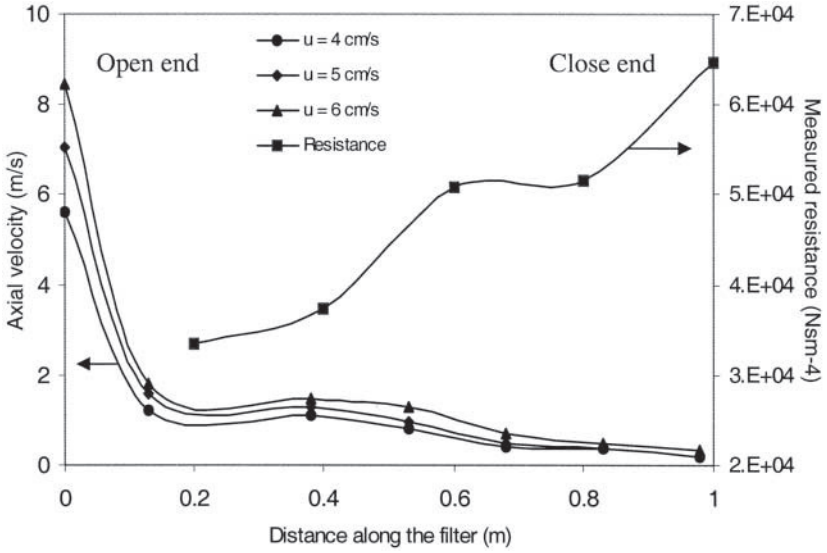

Figure 5. Effect of face velocity on axial velocity with the comparison of filter resistance (u is face velocity).

Figure 5 shows the effect of the face velocity on the axial velocity as measured along the cylindrical filter. At higher face velocities, a higher axial velocity is found in the filter. The dramatic increment in axial velocity started at a distance of 70 cm to 40 cm from the open end and can be explained by the differences in the filter medium resistance along the filter.

A lower resistance was measured at the open end with the resistance increasing toward the closed end. As shown in Fig. 5, the resistance is much higher at a distance of more than 50 cm from the open end. Higher resistance reduces the flow through the filter wall, hence, a lower axial velocity is measured. It has been shown that the filter resistance has a strong influence on the axial velocity profiles, hence, on the pressure gradient. The increment in axial velocity was also caused by the increment of pressure difference across the candle wall towards the open end.

Local Face Velocity Distribution

Figure 6 shows the local face velocity distribution in comparison with the filter resistance during filtration. The local face velocity was calculated from Eq. (11) with the measured local pressure difference across the filter wall and

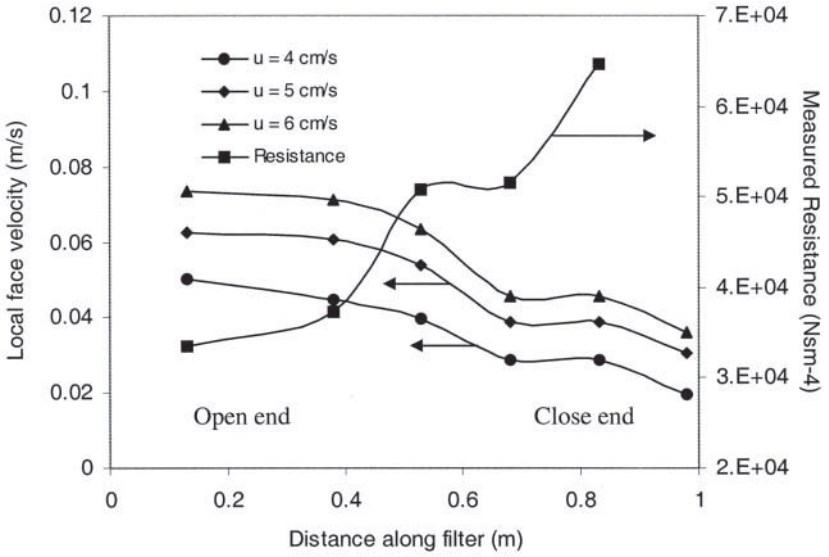

Figure 6. Effect of face velocity on local face velocity with the comparison of filter resistence.

the measured local resistance on the filter sections.

$$U = \frac{(P_o - P)}{\pi D_o R} \tag{11}$$

The local face velocity increased from the closed end of the filter to the open end of the filter, as expected it was noticed that at the closed end the resistance was higher.

Effect of Face Velocity on Pressure Difference Along Filter Axis

Figure 7 shows the effect of the face velocity on the pressure difference between the filter axis and the outside of the filter (atmosphere) at different points along a cylindrical filter. It can be seen that the pressure difference is not constant along the length of the filter element. It decreases from the open end towards the closed end. Figure 7 also shows that the axial pressure difference is smaller than the pressure difference across the filter.

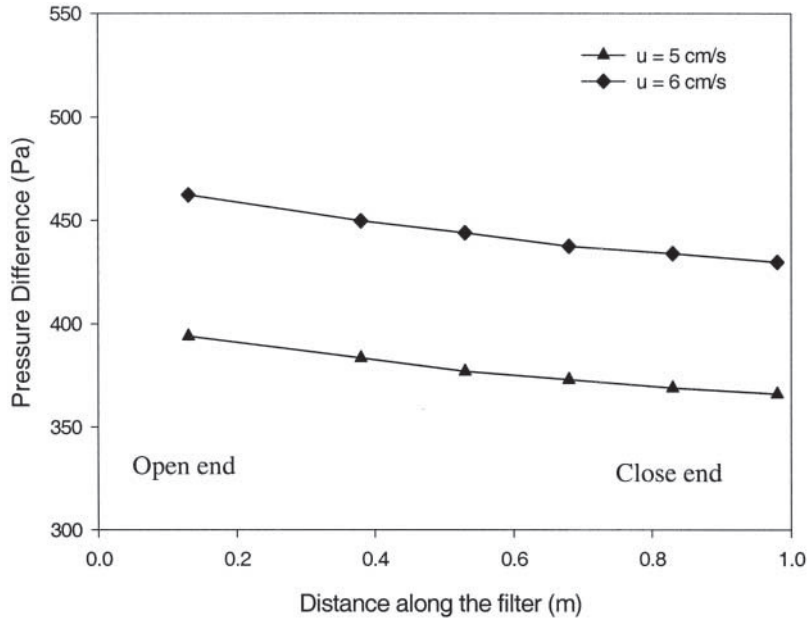

Figure 7. Effect of the face velocity on the pressure difference across the wall in the cylindrical filter.

FILTRATION USING TAPERED FILTERS

All the experimental work presented so far concerned cylindrical filter candles of uniform internal and external diameter. This is a common geometry for filter candles used in industry. However, Withers[20] proposed a design for a conical or "tapered" filter element that may have a more even pressure difference distribution along the filter axis. A schematic diagram of this design is shown in Figs. 3(a) and (b). The filter is longer than the conventional 1.0 m elements by 25 cm. It has an external filtration surface area of 0.32 m^2—68% greater than a 1.0 m element (with an external diameter of 6 cm). The distribution of the internal pressure along the filter during pulse jet cleaning is the main concern and might be influenced by the geometry. It is believed that the high over pressures experienced at the closed end of the filter during pulse jet cleaning can be avoided and the pressure difference more uniformly distributed along the candle length with a conical geometry.

Stephen[21] made a comparison of the tapered filter (named as "Withers" in Fig. 8) and Cerel and Highcron filters using a 1-D model. His findings (Fig. 8) predicted that the internal cleaning pressure can be more evenly dis-

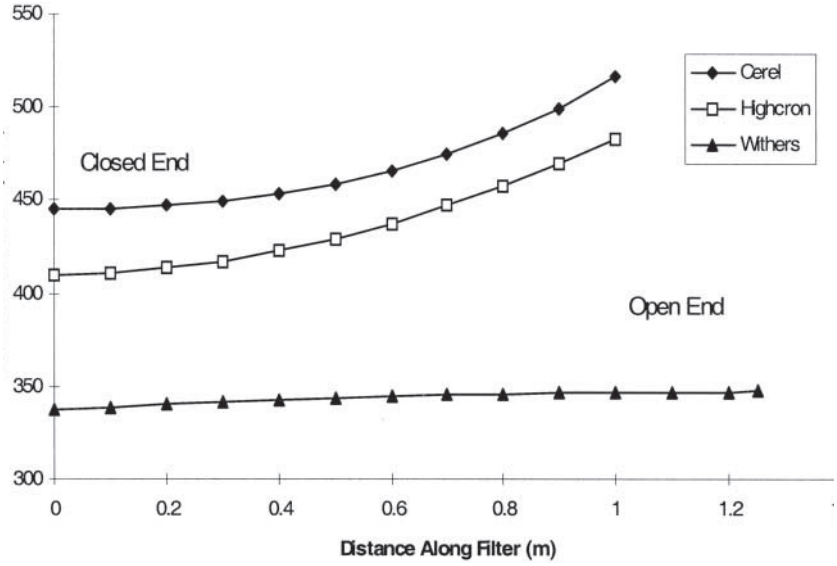

Figure 8. Comparison of the local velocity for tapered and cylindrical elements, the calculated results by Stephens.[21]

tributed using a tapered filter. To validate and to confirm this theory, experiments were carried out as described later.

Effects of Face Velocity on the Pressure Difference in a Tapered Filter

Figure 9 shows the local pressure difference along the length of the tapered filter during filtration. It can be seen, as predicted, that there is a more uniform pressure difference distribution along the filter. As the internal diameter of the filter gets larger towards the open end, the volume of gas injected through the wall of the filter increases (Fig. 10).

In this case, unlike cylindrical filters, the changes of axial velocity are relatively small resulting in little change in the local pressure drop over the wall. However, the local pressure drop in all cases increased by $\sim$15%, not the 2.5% predicted by Stephen.[21] In Stephen's simulation, a larger inner diameter of filter at the open end (10 cm instead of 7.2 cm in the experimental rig) was used. This may result in a more even pressure drop distribution with more flow through the filter at the open end and smaller changes in the pressure difference. The axial velocity is almost constant along the filter element.

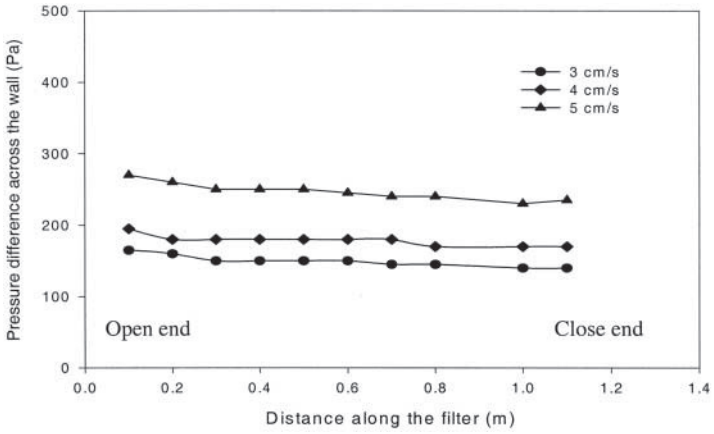

Figure 9. Effect of the face velocity on the pressure difference across the wall in the tapered filter.

Comparison Between Cylindrical and Tapered Filters During Filtration

Figure 11 shows the comparison between the cylindrical filter and the tapered filter during filtration. The tapered filters have approximately a 60% lower pressure drop than do cylindrical filters at a face velocity of 4 cm/s.

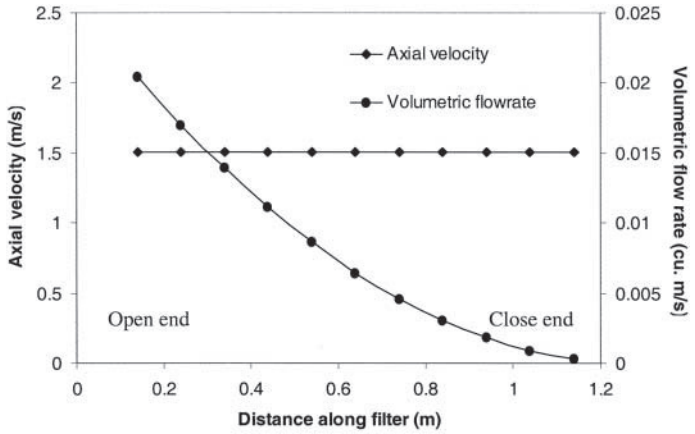

Figure 10. Volumetric flow rate and axial velocity profile of the tapered filter with a face velocity, 3 cm/s.

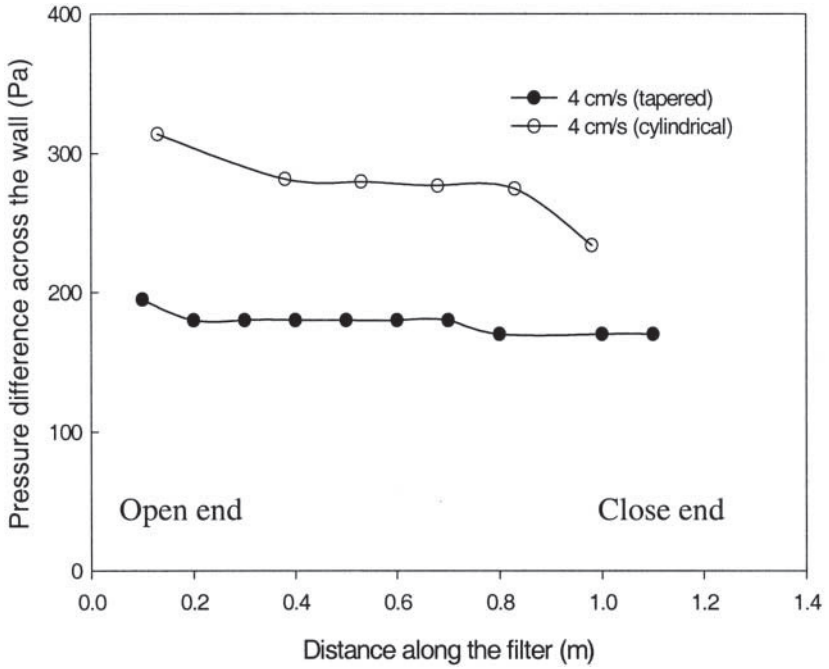

Figure 11. Comparison between the cylindrical and the tapered filters on the pressure difference during filtration (face velocity 4 cm/s).

The axial velocity profile is considered to be "consistent" with position and relatively little changes compared with the cylindrical filter. The local pressure difference over the filter wall increased by only 14% compared with 34% for the cylindrical filter.

The nonuniformity in pressure difference across the wall seen in the cylindrical filters is because of the internal (axial) pressure drop due to both axial momentum changes caused by flow through the wall and the wall friction. Both these effects can be reduced by reducing the axial gas velocity, which can be done by tapering the filter from the open to the close end.

REVERSE FLOW CLEANING ANALYSIS

Previously published data on the flow characteristics during reverse pulsing revealed that the reverse pulse pressure is not usually uniformly distributed along the filter element.[6,8] It is generally agreed that the pressure

is greatest at the closed end of the candle and at a minimum, or even close to zero, at the open end, as shown in Fig. 12. To achieve better cleaning of the filter, it is important to understand the flow field information, especially the gas velocity profile and pressure difference across the filter.

Using the Bernoulli equation, the axial momentum balance is given by Eq. (12):

$$\frac{dP}{dz} + \frac{1}{2}\frac{d}{dz}(\rho u_z^2) = 0 \tag{12}$$

The density term, ρ, can be taken to be constant in the filter cavity (incompressible flow). The axial position along the filter is z and u is the axial velocity.

When permeation of gas through the filter wall does not occur, ρu_z^2 is constant (as in conventional pipe flow) and the pressure will decrease along the filter axis. However, in cleaning, the axial velocity is decreased throughout the filter as the gas permeates from the cavity to the outside of the filter.

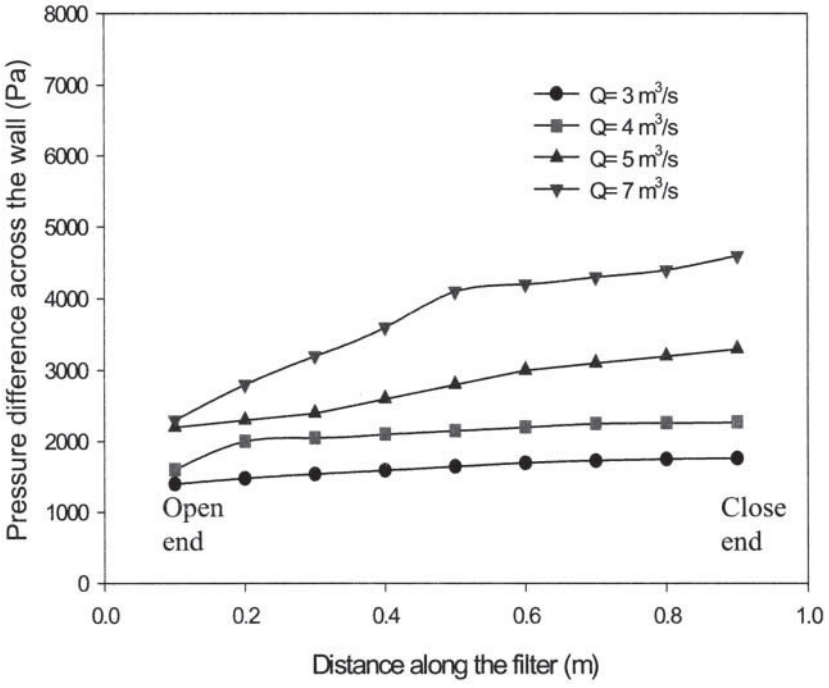

Figure 12. Effect of the reverse flow rate on the pressure difference distribution in a cylindrical filter.

Thus, the second term in the left-hand side of Eq. (12), ρu_z^2, becomes smaller and the pressure difference increases along the filter axis.

Figure 12 shows the pressure difference increased monotonically from the open end to the end of the filter as predicted by Ushiki and Tien.[22] However, at higher gas velocities, Stephen.[21] saw a maximum in pressure difference profile, his finding shows that it is important to include the friction term. Equation (12) can be rewritten to include the effect of the friction factor:

$$> \frac{\mathrm{dP}}{\mathrm{dz}} + \frac{1}{2}\frac{\mathrm{d}}{\mathrm{dz}}(\rho u_z^2) = -4\frac{f}{\mathrm{D_i}}\frac{1}{2}\rho u_z^2 \tag{13}$$

Comparison between Cylindrical and Tapered Filters in Reverse Flow Cleaning

Figure 13 shows the pressure difference distribution along the axis of the tapered filter. It can be seen that there is little change in the local pressure drop across the filter candle wall.

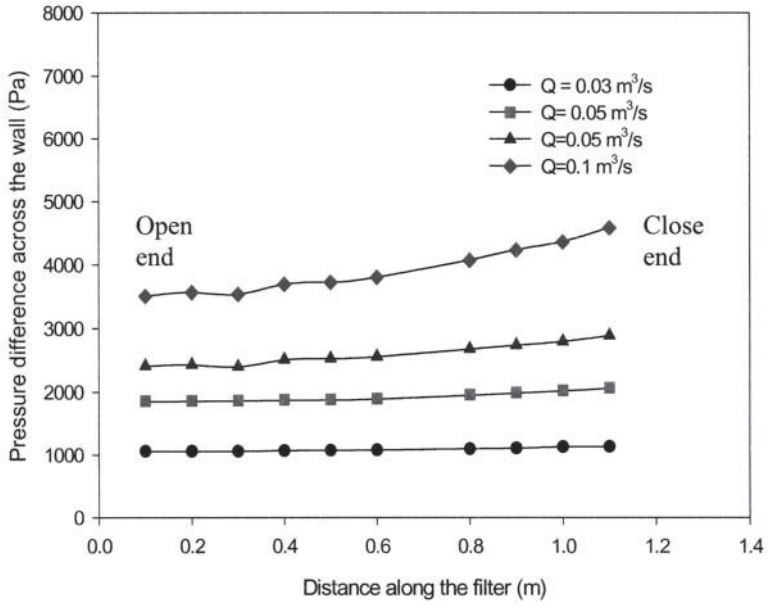

Figure 13. Effect of the reverse flow rate on the pressure difference distribution in the tapered filter.

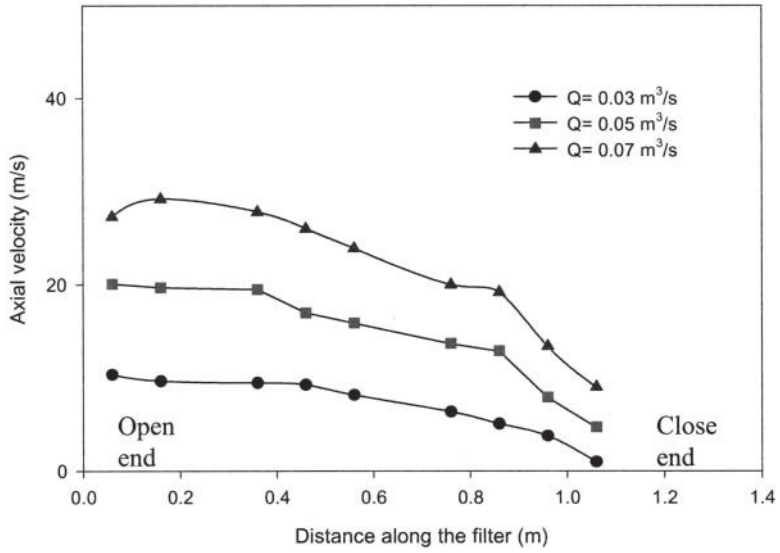

Figure 14. Effect of the reverse flow rate on the axial velocity profile in the tapered filter.

Figure 14 shows the axial velocity profile along the tapered filter axis. The change in axial velocity is smaller than that in the case of the cylindrical filter. Reducing surface area toward the closed end reduces the gas flow from permeating through the filter wall, thus, the pressure difference across the wall does not increase as much in the cylindrical filter.

Comparison of the cylindrical and taper filters is shown in Fig. 15. It is clearly seen that at the same reverse flow rate, the pressure difference across the wall increased significantly for the cylindrical filters. However, for the tapered filters the pressure difference distribution is more uniform along the axis. It can be said that a tapered filter provides a more uniform cleaning pressure and would, therefore, be expected to have more uniform filter cake detachment.

CONCLUSION

This section reported on experiments conducted to investigate the pressure drop and the velocity profile along a filter element for both filtration and reverse flow cleaning modes. Both the filtration and reverse flow cleaning results suggest that a more uniform pressure distribution and axial velocity profile were found in tapered elements.

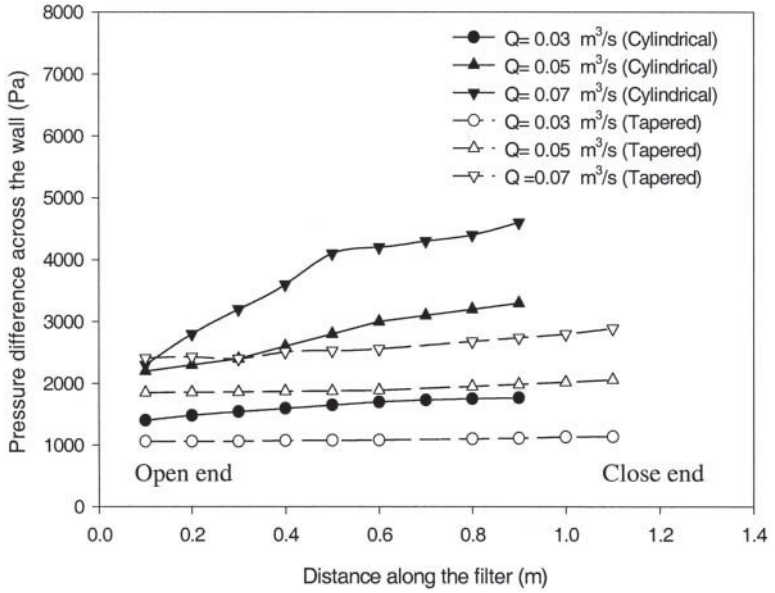

Figure 15. Comparison between cylindrical and tapered filters on the pressure difference across the wall at different reverse flow rates.

The origin of nonuniformity in pressure difference across the wall, in both the filtration and cleaning modes, is internal (axial) pressure drop due to (a) axial momentum changes caused by flow through the wall and (b) wall friction. Both these effects can be reduced by reducing the axial gas velocity, which obviously takes its highest value towards the open end (in both filtration and cleaning modes). This can be done by tapering the filter from the open to the close end.

APPENDIX

Filter Resistance Test

It was vital that a thorough experimental investigation of filter resistance should be carried out. For this purpose, an experimental rig to test the permeability of filter sections was constructed. Figure A.1 shows a schematic diagram of this simple experimental rig was used to investigate the resistance to flow and permeability of individual sections of cylindrical candles.

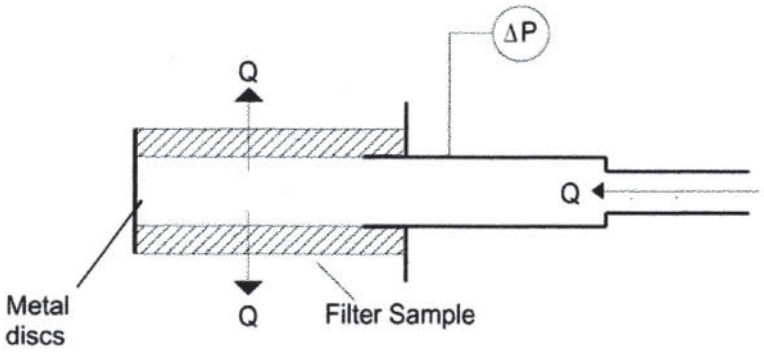

Figure A.1 Experimental rig to test the permeability of filter sections.

The filter candles were cut into short 20 cm sections and placed on the metal holder. The section was sealed with a metal disc at one end and a silicone based sealant at both ends to form an impermeable barrier.

A measured volumetric gas flow was introduced through the open end of the filter and the pressure drop to atmosphere was recorded for a given flowrate. For a short filter candle, the pressure drop in the axial direction is negligible in comparison to that across the wall. For this reason, the rise in pressure drop is linear with velocity. The pressure drop for a typical section of a Cerafil XS-1000 is shown in Fig. A.2.

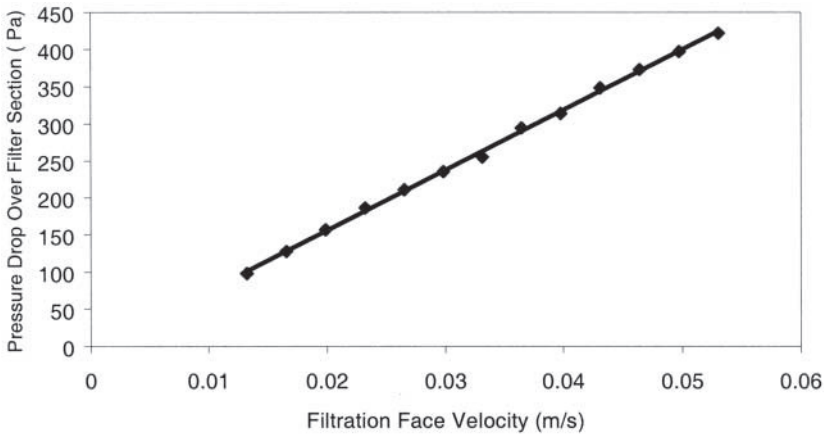

Figure A.2 Pressure rises over 20 cm on Cerafil XS-1000 filter section.

The filtration face velocity is calculated as the volumetric flow divided by the external surface area of the filter section. The resistance to flow of the filter section is determined using the Darcy equation for flow through a porous medium (Eq. A.1). The resistance for the section is calculated from the gradient of plots of pressure drop vs. filtration face velocity.

$$-\frac{dP}{dz} = k_1 \mu U \tag{A.1}$$

NOMENCLATURE

C	discharge coefficient of the orifice plate (−)
D_i	filter inner diameter (m)
D_o	filter outer diameter (m)
D_{pipe}	diameter of pipe (m)
d_o	orifice diameter (m)
f	Fanning friction factor
k_1	filter resistance
L	length of the filter (m)
L_1, L'_2	parameters in Eq. (9)
N	number points of traverse
n	n = 1, 2, 3, . . . N/2 in Eq. (1)
R	filter candle inner radius (m)
Re	Reynold number
r_n	traverse radius (m)
P	pressure (Pa)
$\bar{\Delta}P$	average of the dynamic pressure at the corss section determined by traversing (Pa)
ΔP_o	normalized pressured drop (Pa)
$\Delta P_{orifice}$	pressure drop over orifice (Pa)
Q	actual volumetric flow rate ($m^3\,s^{-1}$)
R	specific resistance (m^{-1})
U	superficial gas velocity ($m\,s^{-1}$)
u_z	gas velocity in z-direction (ms^{-1})
ν	average velocity (ms^{-1})
$\bar{v}$	average velocity (ms^{-1})
z	incremental distance (m)

Greek

β	d_o/D_{pipe}
ρ	fluid density ($kg\,m^{-3}$)

ε_1	expendsibility factor
μ	fluid viscosity (kd $m^{-1}s^{-1}$)

REFERENCES

1. Environmental Quality (Clean Air) Regulation. Malaysia, **1978**, Department of Environmental Engineering (DOE), Malaysia, Kuala Lumpur.
2. Seville, J.P.K.; Clift, R. Gas Cleaning at High Temperatures: Gas and Particle Properties. In *Gas Cleaning in Demanding Applications*; Seville, J.P.K., Ed.; Blackie Academic and Professional: Glasgow, 1997; 1–14.
3. Seville, J.P.K.; Clift, R.; Withers, C.J.; Keidel, W. Rigid ceramic media for filtering hot gases. Filtration and Separation **1989**, *26* (3), 265–271.
4. Seville, J.P.K. Rigid Ceramic Filters. In *Gas Cleaning in Demanding Applications*; Seville, J.P.K., Ed.; Blackie Academic and Professional: Glasgow, 1997; 96–129.
5. Ito, S. Pulse Jet Cleaning and Internal Flow in a Large Ceramic Tube Filter. In *Gas Cleaning at High Temperatures*; Clift, R., Seville, J.P.K., Eds.; Blackie Academic & Professional: Glasgow, 1993; 266–279.
6. Stephen, C.M.; Grannell, S.K.; Seville, J.P.K. Conditioning and Pulse-Cleaning of Rigid Ceramic Filters. In *High Temperature Gas Cleaning*; Schmidt, E., Gäng, P., Pilz, T., Dittler, A., Eds.; Institut für Mechanische Verfahrenstechnik und Mechanik der Universität Karlsruhe: Karlsruhe, 1996; 207–218.
7. Mai, R.; Fronhöfer, M.; Leibold, H. Recleaning of Filter Candles by Fast Pressure Decrease on the Raw Gas Side. In *Separation of Particles from Gases*. Proceeding of 3rd European Symposium PARTEC 95, March 21–23, 1995; Nürnberg, Germany, 301–310.
8. Mai, R.; Fronhöfer, M.; Leibold, H. Flow Charcteristics of Filter Candles During Recleaning. In *High Temperature Gas Cleaning*; Schmidt, E., Gäng, P., Pilz, T., Dittler, A., Eds.; Institut für Mechanische Verfahrenstechnik und Mechanik der Universität Karlsruhe: Karlsruhe, 1996, 194–206.
9. Berbner, S.; Löffler, F. Pulse Jet Cleaning of Rigid Ceramic Filter Elements at High Temperatures. In *Gas Cleaning at High Temperatures*; Clift, R., Seville, J.P.K., Eds.; Blackie Academic & Professional: Glasgow, 1993; 225–243.
10. Hajek, St.; Peukert, W. Experience with High Temperature Filter Media. In *Separation of Particles from Gases*. Proceeding of 3rd European Symposium PARTEC 95, March 21–23, 1995; Nürnberg, Germany, 75–86.
11. Ito, S.; Tanaka, T.; Kawamura, S. Changes in pressure loss and face velocity of ceramic candle filters caused by reverse cleaning in hot coal gas filtration. Powder Technology **1998**, *100*, 32–40.

12. Baik, S.M.; Cheung, C.M.; Biffin, M. Velocity Measurements in Ceramic Candle Filter Elements. In *Environmental Engineering*. Proceeding of First International Conference of Environmental Engineering, Sept 21–23, 1993, De Montfort University, Leicester, U.K., 1993.
13. Christ, A.; Renz, U. Numerical Simulation of Single Ceramic Filter Element Cleaning. In *High Temperature Gas Cleaning*; Schmidt, E., Gäng, P., Pilz, T., Dittler, A., Eds.; Institut für Mechanische Verfahrenstechnik und Mechanik der Universität Karlsruhe: Karlsruhe, 1996, 728–739.
14. Biffin, M.; Panagiotidis, P.; Pitsillides, C. Velocity measurements in a ceramic filter element undergoing pulse cleaning. Proceeding of the Institute of Mechanical Engineers, Part E. J. Process Mechanical Engineering **1997**, *211* (E1), 11–16.
15. Clift, R.; Seville, J.P.K.; ter Kuile, J.W.W. Aerodynamic Considerations in Design and Cleaning of Rigid Ceramic Filters for Hot Gases. In *Proceeding of Vth World Filtration Congress*, Nice, June 5–8, 1990, 530–537.
16. Perry, R.H.; Green, D.W. *Perry Chemical Engineers' Handbook*, 6th Ed.; McGraw-Hill: New York, 1984, 5–9 to 5–11, 5–22.
17. British Standard BS 1042. Measurement of Fluid Flow in Closed Conduits. Section 2.1: Chapter 10.1.1, 1983.
18. ISO 5167-1: 1991 (E). Measurement of Fluid Flow by Means of Pressure Differential Devices. Part 1: Orifice plates, nozzles and venturi tubes inserted in circular cross-section conduit running full.
19. Schiftner, R. Conditioning of a Rigid Ceramic Filter Candle. University of Erlangen-Nürnberg: Germany, 1990; Studienarbeit Thesis.
20. Withers, C.J. Private communication. 1999.
21. Stephen, C.M. Filtration and Cleaning Behaviour of Rigid Ceramic Filters. University of Surrey, 1997; Ph.D. Thesis.
22. Ushiki, K.; Tien, C. Analysis of filter candle performance. Powder Technology **1989**, *58*, 243–258.

Received January 6, 2004
Accepted August 17, 2004